Ultrastrong light-matter coupling of cyclotron transition in monolayer MoS_2

Benliang Li,[1,2] Tao Liu,[1] Daniel W. Hewak,[2] Zexiang Shen,[3] and Qi Jie Wang[1,3,*]

[1]*Centre for OptoElectronics and Biophotonics (COEB), School of Electrical & Electronic Engineering & The Photonics Institute, Nanyang Technological University, 50 Nanyang Ave., Singapore, 639798*

[2]*Optoelectronics Research Centre, University of Southampton, Southampton SO17 1BJ, United Kingdom*

[3]*Centre for Disruptive Photonic Technologies (CDPT), School of Physical and Mathematical Sciences, The Photonics Institute, Nanyang Technological University, Singapore, 637371*

(Received 5 July 2015; revised manuscript received 23 December 2015; published 22 January 2016)

The light-matter coupling between cyclotron transition and photon is theoretically investigated in a monolayer MoS_2 system with consideration of the influence of electron-hole asymmetry. The results show that ultrastrong light-matter coupling can be achieved at a high filling factor of Landau levels. Furthermore, we show that, in contrast to the case for conventional semiconductor resonators, the MoS_2 system shows a vacuum instability. In a monolayer MoS_2 resonator, the diamagnetic term can still play an important role in determining magnetopolariton dispersion, which is different from a monolayer graphene system. The diamagnetic term arises from electron-hole asymmetry, which indicates that electron-hole asymmetry can influence the quantum phase transition. Our study provides new insights in cavity-controlled magnetotransport in the MoS_2 system, which could lead to the development of polariton-based devices.

DOI: 10.1103/PhysRevB.93.045420

I. INTRODUCTION

The strong interaction between an exciton and cavity photon in a high-finesse microcavity can induce a hybrid light-matter eigenstate, which is usually named as polariton in solid-state systems [1]. This strong light-matter interaction can be achieved when this interaction is larger than all broadenings caused by other various factors, e.g., electron phonon scattering and cavity loss. The polariton is now stimulating tremendous research interests due to its high potential in cavity quantum electrodynamics (QED) [2] and the achievement of polaritonic devices. Moreover, when the interaction strength between an excitation and the cavity photon, quantified by vacuum Rabi frequency, becomes comparable to or larger than the corresponding electronic transition frequency in a cavity, the system can enter an ultrastrong coupling regime, which has been experimentally observed [3,4]. In this regime, the standard rotating-wave approximation is no longer valid, and the antiresonant term of the interaction Hamiltonian starts to play an important role, giving rise to exciting effects in cavity QED [5,6].

The discovery of graphene has attracted a great deal of investigations into two-dimensional (2D) materials due to a wide range of extraordinary electrical, optical, mechanical, and thermal properties [7]. Recently, it has been predicted that graphene can enter the ultrastrong light-matter coupling regime under perpendicular magnetic field. In particular, a vacuum instability (phase transition) analogous to the one occurring in the Dicke model can also occur for graphene in this ultrastrong coupling regime, which is absent in the case of massive electrons in semiconductors [8,9]. In addition to graphene, monolayer group VI transition-metal dichalcogenides (e.g., MoS_2, $MoSe_2$, and WS_2) have emerged as a new class of 2D materials, which are being widely investigated due to strong photoluminescence, excellent optical and electric properties, and controllable valley polarization [10–22]. They have a direct bandgap in the visible range, which is located at the K and K' points situated at the corners of the hexagonal first Brillouin zone. The inversion symmetry is explicitly broken into monolayer MoS_2 and other transition-metal dichalcogenides (TMDs), giving rise to a valley-contrasting optical selection rule, which allows optical pumping of valley-polarized carriers by circularly polarized light [23]. Due to their unique properties, MoS_2 and other TMDs have attracted great interest in the study of light-matter interactions. The strong light-matter coupling between an exciton and photon has been experimentally observed recently [24]. One important open question is whether MoS_2 and other TMDs systems can enter the ultrastrong coupling regime and whether a quantum phase transition (or vacuum instability) can occur.

In this paper, we theoretically study the ultrastrong light-matter coupling in a monolayer MoS_2 system under a perpendicular magnetic field with the consideration of electron-hole asymmetry. We show that the ultrastrong light-matter coupling can be achieved at a high filling factor of Landau levels (LLs) and the vacuum instability occurs, which was absent in conventional semiconductor resonators [5,25]. The paper is organized as follows. In Sec. II, we derive the coupling between a cavity resonator and cyclotron transition and establish the second quantized light-matter Hamiltonian for a MoS_2 system based on quantum field theory. At the same time, the electron-hole asymmetry is also considered. In Sec. III, we analyze the results, which show that an ultrastrong light-matter coupling can be achieved at a high filling factor. Furthermore, we show that, in spite of diamagnetic term A_{em}^2, the MoS_2 system still shows a vacuum instability, which is in contrast to the case for conventional semiconductor resonators. Finally, the conclusions are given in Sec. IV.

II. PHYSICAL SYSTEM AND INTERACTION HAMILTONIAN

For the monolayer MoS_2 system, without an external field applied, the conduction and valence band edges are located

*Email address: qjwang@ntu.edu.sg

at the two corners (i.e., K and K') of the first Brillion Zone. The first-principle calculation has shown that the main contributions to band edges near K and K' can be attributed to d_{z^2}, d_{xy}, and $d_{x^2-y^2}$ orbitals of metal atoms and the low-energy band model has been constructed by using the $k \cdot p$ model [26–28]. Ignoring the trigonal warping effect, which can only provide small perturbation terms [29,30], we can write the two band Hamiltonian as [29,31]

$$H_{\tau s} = t_0 a_0 \boldsymbol{k} \cdot \boldsymbol{\sigma}_{\boldsymbol{\tau}} + \frac{\Delta}{2}\sigma_z + \lambda\tau s\frac{1-\sigma_z}{2} + \frac{\hbar^2|\boldsymbol{k}|^2}{4m_0}(\alpha+\beta\sigma_z), \tag{1}$$

where the final term indicates the electron-hole asymmetry. In Eq. (1), m_0 is the free electron mass, $s = \pm$ indicates spin up and down, respectively; and $\tau = \pm$ indicates K and K' valley, respectively, with Pauli matrices $\sigma_\tau = (\tau\sigma_x, \sigma_y)$ and Bloch wave vector $\boldsymbol{k} = (k_x, k_y)$. The energy gap $\Delta = 1.9\,\text{eV}$, and the spin orbit coupling coefficient $\lambda = 80\,\text{meV}$. The other parameters are $t_0 = 1.68\,\text{eV}$, $\alpha = 0.43$, $\beta = 2.21$, and $a_0 = 1.84\,\text{Å}$ [29].

When a perpendicular magnetic field $\boldsymbol{B} = \nabla \times \boldsymbol{A}_0$ is applied to the MoS_2 plane, the electrons occupy highly degenerate LLs. Within the limit $a_0/l_B \ll 1$, we can make the Landau-Peierls substitution $\boldsymbol{k} \to \boldsymbol{k} + e\boldsymbol{A}_0/\hbar$ to the Hamiltonian $H_{\tau s}$, where $l_B = \sqrt{\hbar/(eB)}$ is the magnetic length. Using the Landau gauge $\boldsymbol{A}_0 = (0, Bx, 0)$ and writing the wave function in K valley as

$$\phi_{n,k} = (a_n|n-1,k\rangle, b_n|n,k\rangle), n > 0 \tag{2}$$

$$\phi_{n=0,k} = (0, |0,k\rangle), n = 0 \tag{3}$$

with

$$a_n = \left(i\frac{\sqrt{2}}{l_B}a_0 t_0\sqrt{n}\right)/N_o \tag{4}$$

$$b_n = \left[\frac{\Delta}{2} + \frac{\hbar^2}{2m_0 l_B^2}\left(n-\frac{1}{2}\right)(\alpha+\beta) - E_{n,\tau=+}\right]/N_o, \tag{5}$$

$a_n a_n^* + b_n b_n^* = 1$ and N_o is the normalization factor. Note that $|n,k\rangle$ are LL states with quantum numbers n and k. In this paper, we assume the Fermi level is within the conduction band, and the eigenenergies are as follows [29]:

$$E_{n,\tau s} = \sqrt{\left[\frac{\Delta - \lambda\tau s}{2} + \hbar\omega_{cl}\left(\beta n - \frac{\alpha\tau}{2}\right)\right]^2 + 2n\left(\frac{t_0 a_0}{l_B}\right)^2} + \frac{\lambda\tau s}{2} + \hbar\omega_{cl}\left(\alpha n - \frac{\beta\tau}{2}\right), \tag{6}$$

where cyclotron frequency $\omega_{cl} = eB/2m_0$. In this paper, we neglect the valley and spin splitting of LL energies, which are small so as to have negligible effect on our results. Therefore, the LL degeneracy is $n_B = 4eBL^2/h$, where L is the cavity length. The first unoccupied LL index n is determined by the filling factor $v = \rho S/n_B$ (ρ is electron density), where $S = L^2$ is the monolayer MoS_2 surface area. In this paper, for the sake of simplicity, we will consider the case of an integer filling factor v. As we address the coupling between the light and high filling factor of LLs, we have to take into account the system at cryogenic temperature. Therefore, we assume zero temperature in the rest of the calculations of this paper to ensure the cyclotron transition energy is larger than thermal energy.

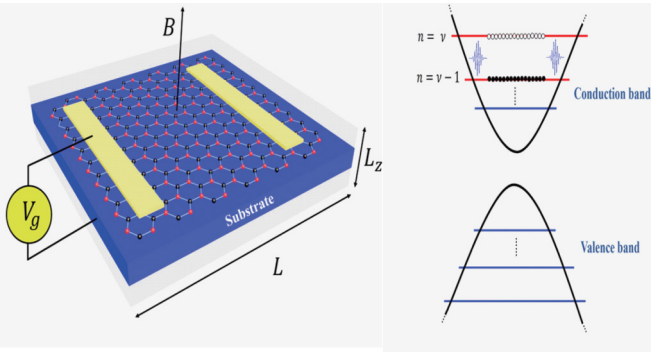

FIG. 1. Left panel: sketch of a cavity resonator embedding a monolayer MoS_2 with a uniform and static magnetic field B applied perpendicularly to the material. Right panel: the MoS_2 cyclotron transition between conduction band LLs $n = v$ and $n = v-1$ is quasiresonant to a confined cavity photon mode.

We consider a rectangular cavity (see Fig. 1) with perfectly conducting walls on all three sides and that has the volume $V = L_z L^2$ with the monolayer MoS_2 material placed at the center of the cavity perpendicular to the z direction. The cavity length L_z along the z direction is assumed to be much smaller than the cavity transverse size L. Therefore, we can restrict our study to the particular photon mode with $n_z = 1$, neglecting all the higher lying modes $n_z > 1$. The electromagnetic vector potential can be written as

$$\boldsymbol{A}_{em}(r) = \sum_{\eta=1,2}\sqrt{\frac{\hbar}{2\varepsilon_0\varepsilon\omega_c V}}\mathbf{u}_\eta(a_\eta + a_\eta^\dagger), \tag{7}$$

where a_η is the annihilation operator for a given photon mode $\eta = 1,2$, ε is the cavity dielectric constant, and $\varepsilon = 4.2$ for the monolayer MoS_2 [32]. Applying the cavity mode with wave vector $\boldsymbol{q} = (q_x, q_y, q_z) = (2\pi/L, 2\pi/L, \pi/L_z)$, the cavity frequency $\omega_c = [\pi c/(L_z\sqrt{\varepsilon})]\sqrt{1+8(L_z/L)^2}$ and the modes can be written as [8,9]

$$u_1 = \begin{pmatrix} 2\cos(2\pi x/L)\sin(2\pi y/L)\cos(\theta) \\ 2\sin(2\pi x/L)\cos(2\pi y/L)\cos(\theta) \\ 0 \end{pmatrix} \tag{8}$$

$$u_2 = \begin{pmatrix} -2\cos(2\pi x/L)\sin(2\pi y/L) \\ 2\sin(2\pi x/L)\cos(2\pi y/L) \\ 0 \end{pmatrix}, \tag{9}$$

where $\cos(\theta) = 1/\sqrt{1+8(L_z/L)^2}$.

Following the procedure of LL bosonization [8,9], we obtain the bosonic bright mode annihilation operator between the transitions $v \to v-1$ coupled to cavity modes $\eta = 1,2$ with the consideration of the condition $|q|l_B \ll 1$ (for the photonic wave vector, this condition is always

satisfied)

$$d_1 = \sqrt{\frac{1}{n_B}} \sum_{k,\pm} \sin\left[\frac{2\pi}{L}\left(k \pm \frac{\pi}{L}\right) l_B^2 \mp \frac{\pi}{4}\right] c^\dagger_{v-1,k} c_{v,k\pm 2\pi/L} \tag{10}$$

$$d_2 = \sqrt{\frac{1}{n_B}} \sum_{k,\pm} \sin\left[\frac{2\pi}{L}\left(k \pm \frac{\pi}{L}\right) l_B^2 \pm \frac{\pi}{4}\right] c^\dagger_{v-1,k} c_{v,k\pm 2\pi/L}, \tag{11}$$

where $c_{v,k}(c^\dagger_{v,k})$ are the annihilation (creation) operators for the eigenstates $\phi_{v,k}$ defined in Eq. (2). Note that d_η ($\eta = 1,2$) are bosonic operators and they satisfy the commutation relation in the ground state and dilute regime as $[d_\eta, d^\dagger_{\eta'}] = \delta_{\eta,\eta'}$.

Starting from the bosonic bright mode operators, after some calculations, we can get the following bosonized version of the kinetic part H_L, the light-matter interaction part $H_{\rm int}$, and the diamagnetic term $H_{\rm dia}$ as (see Appendix)

$$H_L = \sum_{\eta=1,2} \hbar\omega_{eg} d^\dagger_\eta d_\eta \tag{12}$$

$$H_{\rm int} = \sum_{\eta=1,2} \hbar\Omega_\eta (d_\eta + d^\dagger_\eta)(a_\eta + a^\dagger_\eta) \tag{13}$$

$$H_{\rm dia} = \sum_{\eta=1,2} \hbar D_\eta (a_\eta + a^\dagger_\eta)^2, \tag{14}$$

where $\Omega_1 = \Omega_2 \cos(\theta), D_1 = D_2 \cos^2(\theta)$ and the vacuum Rabi frequency of mode two ($\eta = 2$) is

$$\Omega_2 = \sqrt{\frac{1}{2\hbar\varepsilon_0\varepsilon\omega_c V}} \frac{i\sqrt{2} a^*_v b_{v-1} a_0 t_0 e\sqrt{n_B}}{\hbar} + \sqrt{\frac{1}{2\hbar\varepsilon_0\varepsilon\omega_c V}} \frac{e\hbar\sqrt{n_B}}{2m_0 l_B} [(\alpha+\beta) a^*_{v-1} a_v \sqrt{v-1} + (\alpha-\beta) b^*_{v-1} b_v \sqrt{v}], \tag{15}$$

and transition frequency ω_{eg} between nearby LLs and diamagnetic terms D_2 are

$$\omega_{eg} = (E_v - E_{v-1})/\hbar \tag{16}$$

$$D_2 = \frac{n_B e^2}{4\varepsilon_0\varepsilon\omega_c m_0 V} \sum_{n=0}^{v-1} [a^*_n a_n (\alpha+\beta) + b^*_n b_n (\alpha-\beta)]. \tag{17}$$

Note that in monolayer MoS_2, similar to graphene, a quantum critical value exists because $D_2\omega_{eg}$ is smaller than Ω_2^2, e.g., with $v = 50$ and $B = 1T$, $D_2\omega_{eg}/\Omega_2^2 \approx 0.5$ [8,33]. Above this critical value, a spontaneous coherence of light and matter appears. The ground state becomes twice degenerate, and the system goes into super-radiant quantum phase. In addition to the light-matter interaction, we should also include the Coulomb interaction, which plays an important role. We can only consider the Coulomb interaction between transition $v-1$ and v levels. Based on our cavity structure, it is straightforward that the Coulomb potential $V(r-r')$ should be expanded in terms of the 2D Fourier series. By the

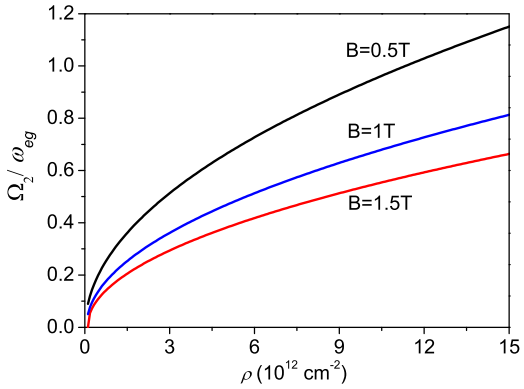

FIG. 2. The dimensionless vacuum Rabi frequency Ω_2/ω_{eg} versus the doping density ρ. Other parameters are $L_z = 1$ mm, $L = 8L_z$, and $\omega_c = 0.49\,\mathrm{THz\,rad^{-1}}$. ω_{eg} is the cyclotron transition frequency between the last occupied LL with the first unoccupied one.

bosonization of the Coulomb Hamiltonian, we find

$$H_{\rm Coul} = \sum_{\eta=1,2} \hbar V_c \chi_\eta (d_\eta + \chi_\eta d^\dagger_\eta)^2, \tag{18}$$

where $\chi_1 = -1$, $\chi_2 = 1$, and

$$V_c = \frac{n_B e^2 l_B^2 v\pi}{8\sqrt{2}\varepsilon_0\varepsilon L^3\hbar} \left(a^*_v a_{v-1}\sqrt{\frac{v-1}{v}} + b^*_v b_{v-1}\right)^2. \tag{19}$$

By diagonalizing the kinetic and Coulomb Hamiltonian, we can obtain the magnetoplasmon modes

$$H_{\rm Coul} + H_L = \sum_{\eta=1,2} \hbar\omega_p g^\dagger_\eta g_\eta + \text{const}, \tag{20}$$

where $g_\eta = u_\eta d_\eta + v_\eta d^\dagger_\eta$ is the magnetoplasmon mode, where $\omega_p = \sqrt{\omega_{eg}(\omega_{eg} + 4V_c)}$, $u_\eta = -\chi_\eta \frac{\omega_p + \omega_{eg}}{2\sqrt{\omega_{eg}\omega_p}}$, and $v_\eta = \frac{\omega_{eg} - \omega_p}{2\sqrt{\omega_{eg}\omega_p}}$.

Then, we can write the total Hamiltonian describing photonic and magnetoplasmon modes

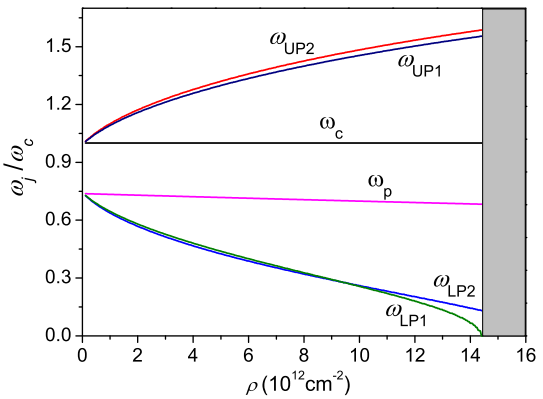

FIG. 3. Normalized frequencies of LP and UP branches of magnetopolariton as a function of doping density for $\eta = 1$ and $\eta = 2$. Parameters are $B = 0.75$ T, $L_z = 1$ mm, $L = 8L_z$, and $\omega_c = 0.49\,\mathrm{THz\,rad^{-1}}$; the critical density for phase transition is $\rho_c = 1.44 \times 10^{13}\mathrm{cm}^{-2}$.

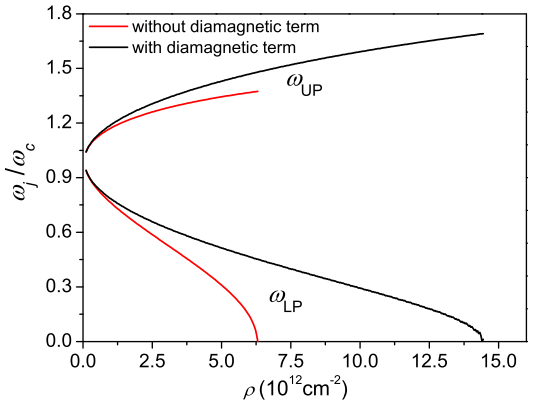

FIG. 4. Normalized frequencies of LP and UP branches of magnetopolariton as a function of doping density with and without the diamagnetic term, e.g., for $\eta = 2$. Parameters are $B = 1\,\mathrm{T}$, $L_z = 1\,\mathrm{mm}$, $L = 8L_z$, and $\omega_c = 0.49\,\mathrm{THz\,rad^{-1}}$; the critical density for phase transition is $\rho_c = 1.44 \times 10^{13}\mathrm{cm}^{-2}$ and $\rho_c = 6.30 \times 10^{12}\mathrm{cm}^{-2}$ with and without diamagnetic terms, respectively.

as

$$H = \sum_{\eta=1,2} [\hbar\omega_p g_\eta^\dagger g_\eta + \hbar\omega_c a_\eta^\dagger a_\eta + \hbar\tilde{\Omega}_\eta (g_\eta^\dagger + g_\eta)(a_\eta + a_\eta^\dagger) + \hbar D_\eta (a_\eta + a_\eta^\dagger)^2], \tag{21}$$

where $\tilde{\Omega}_\eta = (u_\eta - v_\eta)\Omega_\eta$.

Introducing polariton operators $p_{j,\eta} = c_{j,\eta} g_\eta^\dagger + d_{j,\eta} a_\eta^\dagger + e_{j,\eta} g_\eta + f_{j,\eta} a_\eta$, we can write the Hamiltonian (21) in polariton basis as

$$H = \sum_{j,\eta} \hbar\omega_{j,\eta} p_{j,\eta}^\dagger p_{j,\eta} + \text{const.} \tag{22}$$

Here j indicates upper polaritons (UPs) and lower polaritons (LPs), and the commutation relation $[p_{j,\eta}, p_{j',\eta}^\dagger] = \delta_{j,j'}$. By calculating the commutation relation $[p_{j,\eta}, H] = \hbar\omega_{j,\eta} p_{j,\eta}$, we can obtain a 4×4 matrix that can be written as

$$\begin{pmatrix} \omega_c + 2D_\eta & \tilde{\Omega}_\eta & -2D_\eta & -\tilde{\Omega}_\eta \\ \tilde{\Omega}_\eta & \omega_p & -\tilde{\Omega}_\eta & 0 \\ 2D_\eta & \tilde{\Omega}_\eta & -\omega_c - 2D_\eta & -\tilde{\Omega}_\eta \\ \tilde{\Omega}_\eta & 0 & -\tilde{\Omega}_\eta & -\omega_p \end{pmatrix}. \tag{23}$$

By diagonalizing the matrix, we can obtain the eigenfrequency of the polaritons. Meanwhile, the critical value of $\tilde{\Omega}$, beyond which the system may enter super-radiant phase regime, is $\tilde{\Omega}_c = \sqrt{\omega_p(\omega_c + 4D)}/2$. The phase transition occurs at $v = 200$ with $B = 0.75\mathrm{T}$, which we will show below.

III. NUMERICAL RESULTS AND DISCUSSIONS

As written in Eq. (15), we have obtained the vacuum Rabi frequency of the monolayer MoS_2 system, and we then can characterize the intrinsic strength of the transition, i.e., the ratio between vacuum Rabi frequency Ω_2 with LL transition frequency ω_{eg}, which is shown in Fig. 2. The results show that the dimensionless vacuum Rabi frequency Ω_2/ω_{eg} can be comparable to or even larger than 1 for small magnetic field B and large enough doping density. We can conclude that, as is the case for graphene, the monolayer MoS_2 system can also enter the ultrastrong coupling regime. Note that in our paper, the carrier doping is induced by the external electric fields, and their relations can be simply calculated according to Ref. [34]. But as discussed in Ref. [29], the external electric field will also influence the electron-hole asymmetry, thus the band structure of MoS_2. For the sake of simplicity, we adopt the formula used in Ref. [29], which describes the relation between the electron-hole asymmetry and electric field.

Using Eq. (23), we can calculate the magnetopolariton dispersion. In Fig. 3, we show the carrier density dependences of frequencies of magnetopolariton normalized to the cavity mode, where the LP and UP branches are the two spectrally separated light-matter eigenstates in strong coupling regime. In contrast to the conventional semiconductor materials (e.g., GaAs), the monolayer MoS_2 resonator, as a 2D semiconductor material, shows the existence of quantum critical point ($\rho_c = 1.44 \times 10^{13}\mathrm{cm}^{-2}$ in our considered parameter) beyond which the normal ground state becomes unstable. This quantum critical point exits in the MoS_2 system

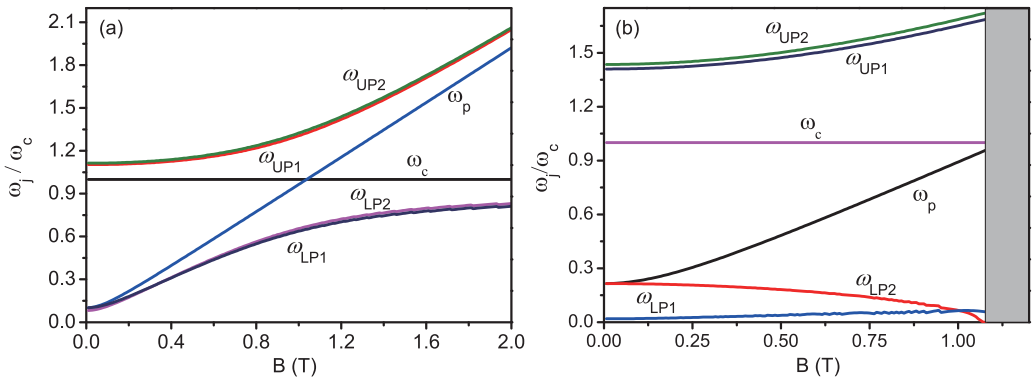

FIG. 5. (a) Normalized frequencies of LP and UP branches of magnetopolariton as a function of magnetic field B, doping density is $\rho = 2.81 \times 10^{12}\mathrm{cm}^{-2}$. (b) Normalized frequencies of LP and UP branches of magnetopolariton as a function of magnetic field B, doping density is $\rho = 1.42 \times 10^{13}\mathrm{cm}^{-2}$, which is just below the critical density. The critical value of magnetic field B for phase transition is $B_c = 1.06\,\mathrm{T}$, beyond which the system may enter the super-radiant phase regime.

due to the smaller diamagnetic term rather than vacuum Rabi frequency term, i.e., $D_2 < \Omega_2^2/\omega_{eg}$, as discussed above [33]. In conventional semiconductors, the diamagnetic term is even dominant in the ultrastrong coupling regime between a cavity resonator and cyclotron transitions.

In contrast to graphene, the diamagnetic term can still play an important role in determining magnetopolariton dispersion for the monolayer MoS_2 system, as shown in Fig. 4. The quantum critical point of the MoS_2 resonator can be greatly increased from $\rho_c = 6.30 \times 10^{12}\text{cm}^{-2}$ to $\rho_c = 1.44 \times 10^{13}\text{cm}^{-2}$ when considering the diamagnetic term. On the other hand, the diamagnetic term arises from the electron-hole asymmetry, which indicates that electron-hole asymmetry can influence the quantum phase transition (see Appendix).

We close the analysis by considering the effect of magnetic field on magnetopolariton at doping density far away from the quantum critical point [Fig. 5(a)] and one just below the critical point [Fig. 5(b)]. As a 2D semiconductor material, the MoS_2 system has a similar magnetic field dependent magnetopolariton dispersion curve with a 2D electron gas in quantum wells if the doping density is far away from the critical density. However, when doping density is just below the critical point, the dispersion curve is very different, as depicted in Fig. 5(b). As the magnetic field increases, a strong asymmetric dispersion is exhibited, which shows the signature of such phase transition.

IV. CONCLUSIONS

In conclusion, we theoretically investigate the cavity QED in a monolayer MoS_2 system under perpendicular magnetic field with the consideration of electron-hole asymmetry. The results show that the MoS_2 system can enter the ultrastrong light-matter coupling regime. But, in contrast to conventional semiconductors, the semiconductor monolayer MoS_2 system shows a quantum phase transition. In the monolayer MoS_2 resonator, the diamagnetic term can still play an important role in determining magnetopolariton dispersion, which is different from the monolayer graphene system. The diamagnetic term arises from electron-hole asymmetry, which indicates that electron-hole asymmetry can influence the quantum phase transition. Our study provides a theoretical foundation for the observation and investigation of cavity QED for fundamental studies and quantum applications in a MoS_2 system.

ACKNOWLEDGMENTS

We thank Hu Xiaonan and Chen Shaoxiang for drawing schematics of the setup. This work is supported by Research Grants MOE2011-T2-2-147 and MOE2011-T3-1-005 from the Ministry of Education, Singapore and partially by Agency for Science, Technology and Research (A*STAR)-Ministry of Defence Singapore (MINDEF) Joint Funding Programme No. 122 331 0076.

APPENDIX

Neglecting the spin and valley splitting effects, the first order Hamiltonian, including the light-matter interaction, can be written as two parts $H_1 = H_{1,L} + H_{1,\text{int}}$, where kinetic energy part reads

$$H_{1,L} = \begin{pmatrix} \frac{\Delta}{2} & 0 \\ 0 & -\frac{\Delta}{2} \end{pmatrix} + a_0 t_0 \begin{pmatrix} 0 & k_x + \frac{eA_{0,x}}{\hbar} - i\left(k_y + \frac{eA_{0,y}}{\hbar}\right) \\ k_x + \frac{eA_{0,x}}{\hbar} + i\left(k_y + \frac{eA_{0,y}}{\hbar}\right) & 0 \end{pmatrix}, \tag{A1}$$

and the light-matter interaction part reads

$$H_{1,\text{int}} = a_0 t_0 \begin{pmatrix} 0 & \frac{eA_{em,x}}{\hbar} - i\frac{eA_{em,y}}{\hbar} \\ \frac{eA_{em,x}}{\hbar} + i\frac{eA_{em,y}}{\hbar} & 0 \end{pmatrix}. \tag{A2}$$

Similarly, the second order Hamiltonian (electron-hole asymmetry term), including the light-matter interaction, can be written as three parts $H_2 = H_{2,L} + H_{2,\text{int}} + H_{\text{dia}}$, where the kinetic energy part reads

$$H_{2,L} = \begin{pmatrix} (\alpha+\beta)\frac{\hbar^2}{4m_0}\left(\boldsymbol{k} + \frac{e\boldsymbol{A}_0}{\hbar}\right)^2 & 0 \\ 0 & (\alpha-\beta)\frac{\hbar^2}{4m_0}\left(\boldsymbol{k} + \frac{e\boldsymbol{A}_0}{\hbar}\right)^2 \end{pmatrix}, \tag{A3}$$

the light-matter interaction part reads

$$H_{2,\text{int}} = \begin{pmatrix} (\alpha+\beta)\frac{\hbar^2}{4m_0}\left[\left(\boldsymbol{k} + \frac{e\boldsymbol{A}_0}{\hbar}\right)\cdot\frac{e\boldsymbol{A}_{em}}{\hbar} + \frac{e\boldsymbol{A}_{em}}{\hbar}\cdot\left(\boldsymbol{k} + \frac{e\boldsymbol{A}_0}{\hbar}\right)\right] & 0 \\ 0 & (\alpha-\beta)\frac{\hbar^2}{4m_0}\left[\left(\boldsymbol{k} + \frac{e\boldsymbol{A}_0}{\hbar}\right)\cdot\frac{e\boldsymbol{A}_{em}}{\hbar} + \frac{e\boldsymbol{A}_{em}}{\hbar}\cdot\left(\boldsymbol{k} + \frac{e\boldsymbol{A}_0}{\hbar}\right)\right] \end{pmatrix}, \tag{A4}$$

and in addition we have the diamagnetic term, which reads

$$H_{\text{dia}} = \begin{pmatrix} (\alpha+\beta)\frac{\hbar^2}{4m_0}\left(\frac{e\boldsymbol{A}_{em}}{\hbar}\right)^2 & 0 \\ 0 & (\alpha-\beta)\frac{\hbar^2}{4m_0}\left(\frac{e\boldsymbol{A}_{em}}{\hbar}\right)^2 \end{pmatrix}, \tag{A5}$$

where $\boldsymbol{A}_0 = (0, Bx, 0)$ and $\boldsymbol{A}_{em}$ is given by Eq. (7). We write the kinetic energy part of the Hamiltonian $H_L = H_{1,L} + H_{2,L}$ in LL basis, which is given by Eq. (2) as $H_L = \sum_{n,k} E_n c_{n,k}^\dagger c_{n,k}$, where E_n is given by Eq. (6) and $c_{n,k}^\dagger$ is the Fermi creation operator for the eigenstates $\phi_{n,k}$ defined in Eq. (2). In order

to bosonize the kinetic Hamiltonian H_L, we calculate the commutation relation $[H_L, d_\eta^\dagger] = \hbar\omega_{eg} d_\eta^\dagger$, where ω_{eg} is shown in Eq. (16) as the transition frequency between nearby LLs, and we obtain the bosonized Hamiltonian H_L, as given by Eq. (12). Next, we give the bosonization procedure for the first order of interaction Hamiltonian $H_{1,\mathrm{int}}$. First, we write $H_{1,\mathrm{int}}$ in LL basis as

$$H_{1,\mathrm{int}} = \sum_{n,n',k,k'} \frac{a_0 t_0 e}{\hbar} [a_{n'} b_n^* \langle n,k|(\boldsymbol{A}_{em,x} + i\boldsymbol{A}_{em,y})|n'-1,k'\rangle + a_n^* b_{n'} \langle n-1,k|(\boldsymbol{A}_{em,x} - i\boldsymbol{A}_{em,y})|n',k'\rangle] c_{n,k}^\dagger c_{n',k'}. \tag{A6}$$

Since we are dealing with low energy cavity modes, the LL mixing can be neglected, and we have $\langle n,k|\exp(-i\boldsymbol{q}\cdot\boldsymbol{r})|n',k'\rangle = \exp(-i\frac{q_x(k+k')l_B^2}{2})\chi_{n,n'}(ql_B)\delta_{k,k'+q_y}$ thanks to the condition $|\boldsymbol{q}|l_B \ll 1$, where $\chi_{n,n'}(ql_B) \equiv \Theta(n-n')G_{n,n'}(q^*l_B) + \Theta(n'-n)G_{n',n}(ql_B)$, $G_{n,n'}(ql_B) = \sqrt{\frac{n'!}{n!}}(\frac{-iql_B}{\sqrt{2}})^{n-n'} \sum_{j=0}^{n'} \frac{n!}{(n'-j)!(n-n'+j)!} \frac{(-|ql_B|^2)^j}{2^j j!}$, $q = q_x + iq_y$, and $\Theta(n)$ is a Heaviside step function. Bearing in mind that we are dealing with the cyclotron transitions between the last occupied LL, $n = v-1$, with the first unoccupied one, $n = v$. Finally, we arrive at

$$H_{1,\mathrm{int}} = \sum_{\eta=1,2} \hbar\Omega_{1,\eta}(d_\eta + d^\dagger)(a_\eta + a^\dagger), \tag{A7}$$

where for the cavity mode two ($\eta = 2$) we obtain the first order of vacuum Rabi frequency, written as the first part of the right-hand side in Eq. (15); the bosonic operator d_η is shown in Eq. (10) and Eq. (11). Similarly, the second order vacuum Rabi frequency can be obtained from Hamiltonian $H_{2,\mathrm{int}}$, and it is shown as the second part of the right-hand side in Eq. (15). The diamagnetic contribution H_{dia} can be bosonized in a similar way, which can be written in form as

$$H_{\mathrm{dia}} = \sum_{n,n',k,k'} \Big[a_{n'} a_n^* (\alpha+\beta) \frac{e^2}{4m_0} \langle n-1,k|\boldsymbol{A}_{em}^2|n'-1,k'\rangle + b_{n'} b_n^* (\alpha-\beta) \frac{e^2}{4m_0} \langle n,k|\boldsymbol{A}_{em}^2|n',k'\rangle \Big] c_{n,k}^\dagger c_{n',k'} \tag{A8}$$

by setting $n = n'$ and $k = k'$, and summing over k provides the LL degeneracy n_B. Replace the number operator $c_{n,k}^\dagger c_{n',k'}$ by the its expectation value $\langle c_{n,k}^\dagger c_{n,k}\rangle = \Theta(v-1-n)$ in the electronic ground state $|F\rangle$ with

$$|F\rangle = \prod_{n=0}^{v-1} \prod_{k=1}^{n_B} c_{n,k}^\dagger |0\rangle. \tag{A9}$$

Finally, we can obtain this diamagnetic term, as shown in Eq. (14).

[1] H. Deng, G. Weihs, D. W. Snoke, J. Bloch, and Y. Yamamoto, Proc. Natl. Acad. Sci. USA **100**, 15318 (2003).

[2] C. Schneider, A. Rahimi-Iman, N. Y. Kim, J. Fischer, I. G. Savenko, M. Amthor, M. Lermer, A. Wolf, L. Worschech, V. D. Kulakovskii, I. A. Shelykh, M. Kamp, S. Reitzenstein, A. Forchel, Y. Yamamoto, and S. Hofling, Nature (London) **497**, 348 (2013).

[3] G. Scalari, C. Maissen, D. Turcinkova, D. Hagenmuller, S. De Liberato, C. Ciuti, C. Reichl, D. Schuh, W. Wegscheider, M. Beck, and J. Faist, Science **335**, 1323 (2012).

[4] G. Gunter, A. A. Anappara, J. Hees, A. Sell, G. Biasiol, L. Sorba, S. De Liberato, C. Ciuti, A. Tredicucci, A. Leitenstorfer, and R. Huber, Nature (London) **458**, 178 (2009).

[5] C. Ciuti, G. Bastard, and I. Carusotto, Phys. Rev. B **72**, 115303 (2005).

[6] S. De Liberato, C. Ciuti, and I. Carusotto, Phys. Rev. Lett. **98**, 103602 (2007).

[7] A. H. Castro Neto, F. Guinea, N. M. R. Peres, K. S. Novoselov, and A. K. Geim, Rev. Mod. Phys. **81**, 109 (2009).

[8] D. Hagenmuller and C. Ciuti, Phys. Rev. Lett. **109**, 267403 (2012).

[9] T. Liu and Q. J. Wang, Phys. Rev. B **89**, 125306 (2014).

[10] K. Mak, K. He, J. Shan, and T. F. Heinz, Nature Nanotech. **7**, 494 (2012).

[11] K. F. Mak, C. Lee, J. Hone, J. Shan, and T. F. Heinz, Phys. Rev. Lett. **105**, 136805 (2010).

[12] A. Splendiani, L. Sun, Y. Zhang, T. Li, J. Kim, C. Y. Chim, G. Galli, and F. Wang, Nano Lett. **10**, 1271 (2010).

[13] Q. H. Wang, K. K. Zadeh, A. Kis, J. N. Coleman, and M. S. Strano, Nat. Nanotechnol. **7**, 699 (2012).

[14] K. F. Mak, K. L. McGill, J. Park, and P. L. McEuen, Science **344**, 1489 (2014).

[15] G. Aivazian, Z. Gong, A. M. Jones, R.-L. Chu, J. Yan, D. G Mandrus, C. Zhang, D. Cobden, W. Yao, and X. Xu, Nature Phys. **11**, 148 (2015).

[16] A. Srivastava, M. Sidler, A. V. Allain, D. S. Lembke, A. Kis, and A. Imamoğlu, Nat. Phys. **11**, 141 (2015).

[17] Y. Li, J. Ludwig, T. Low, A. Chernikov, X. Cui, G. Arefe, Y. D. Kim, A. M. van der Zande, A. Rigosi, H. M. Hill, S. H. Kim, J. Hone, Z. Li, D. Smirnov, and T. F. Heinz, Phys. Rev. Lett. **113**, 266804 (2014).

[18] D. MacNeill, C. Heikes, K. F. Mak, Z. Anderson, A. Kormányos, V. Zóolyomi, J. Park, and D. C. Ralph, Phys. Rev. Lett. **114**, 037401 (2015).

[19] H. Zeng, J. Dai, W. Yao, D. Xiao, and X. Cui, Nature Nanotechnology **7**, 490 (2012).

[20] T. Cao, G. Wang, W. Han, H. Y. C. Zhu, J. Shi, Q. Niu, P. Tan, E. Wang, B. Liu, and J. Feng, Nature Commun. **3**, 887 (2012).

[21] A. M. Jones, H. Yu, N. J. Ghimire, S. Wu, G. Aivazian, J. S. Ross, B. Zhao, J. Yan, D. G. Mandrus, D. Xiao, W. Yao, and X. Xu, Nat. Nanotechnol. **8**, 634 (2013).

[22] J. S. Ross, S. Wu, H. Yu, N. Ghimire, A. Jones, G. Aivazian, J. Yan, D. Mandrus, D. Xiao, W. Yao, and X. Xu, Nature Commun. **4**, 1474 (2013).

[23] D. Xiao, G. B. Liu, W. X. Feng, X. D. Xu, and W. Yao, Phys. Rev. Lett. **108**, 196802 (2012).

[24] X. Liu, T. Galfsky, Z. Sun, F. Xia, E.-C. Lin, Y.-H. Lee, S. Kéna-Cohen, and V. M. Menon, Nat. Photon. **9**, 30 (2015).

[25] D. Hagenmuller, S. De Liberato, and C. Ciuti, Phys. Rev. B **81**, 235303 (2010).
[26] X. Xu, W. Yao, D. Xiao, and T. F. Heinz, Nat. Phys. **10**, 343 (2014).
[27] G. B. Liu, D. Xiao, Y. Yao, X. Xu, and W. Yao, Chem. Soc. Rev. **44**, 2643 (2015).
[28] G. B. Liu, W. Y. Shan, Y. G. Yao, W. Yao, and D. Xiao, Phys. Rev. B **88**, 085433 (2013).
[29] H. Rostami, A. G. Moghaddam, and R. Asgari, Phys. Rev. B **88**, 085440 (2013).
[30] F. Rose, M. O. Goerbig, and F. Piechon, Phys. Rev. B **88**, 125438 (2013).
[31] A. Kormanyos, V. Zolyomi, N. D. Drummond, P. Rakyta, G. Burkard, and V. I. Fal'ko, Phys. Rev. B **88**, 045416 (2013).
[32] T. Cheiwchanchamnangij and W. R. L. Lambrecht, Phys. Rev. B **85**, 205302 (2012).
[33] P. Nataf and C. Ciuti, Nat. Commun. **1**, 72 (2010).
[34] C. P. Lu, G. H. Li, J. H. Mao, L. M. Wang, and E. Y. Andrei, Nano Lett. **14**, 4628 (2014).